Modified TEODI MPPT Technique: Theoretical Analysis and Experimental Validation in Uniform and Mismatching Conditions

Marco Balato, Luigi Costanzo, Pompeo Marino, Guido Rubino, Luigi Rubino, and Massimo Vitelli

***Abstract*—In this paper, the theoretical analysis and the experimental validation of a modified version of the maximum power point tracking technique, that is known with the acronym TEODI, are presented and discussed. The modified version of TEODI (MTEODI) outperforms TEODI in photovoltaic (PV) applications operating under mismatching conditions. The working principle of MTEODI is based on the periodic measurement of the short-circuit currents of the PV units. The knowledge of such currents allows not only the determination of whether mismatching conditions occur but identification of the values of the suitable correction factors, on which the working of MTEODI is based, as well.**

***Index Terms*—Distributed maximum power point tracking (DMPPT), mismatching, performance optimization, photovoltaic (PV).**

I. Introduction

In CENTRALIZED photovoltaic (PV) architectures, a unique central inverter carries out the so-called central maximum power point tracking (CMPPT), that is, the maximum power point tracking (MPPT) function is carried out on the whole PV array [1]. It is well known that, in mismatching operating conditions (due to shadows, debris, manufacturing tolerances, aging, different orientation of parts of the PV field, etc.), PV systems that adopt CMPPT may exhibit a consistent reduction of the energy efficiency [1], [2]. In fact, when mismatching conditions occur, the CMPPT controller may be deceived due to the fact that the power versus voltage (P–V) characteristic of the PV array may exhibit more than one peak (due to bypass diodes conduction and/or reverse bias operation of shaded cells). Under such conditions, the operating point of the PV system may remain trapped in the neighborhood of a relative MPP rather than in the neighborhood of the absolute MPP. Moreover, in mismatching conditions, even if the absolute MPP is correctly identified, the associated power is lower than the sum of the available maximum powers that the mismatched modules are able to provide. Distributed maximum power point tracking (DMPPT) architectures [3]–[6] allow us to reduce mismatching losses. They

Manuscript received July 12, 2016; revised September 16, 2016; accepted October 17, 2016. Date of publication December 16, 2016; date of current version February 16, 2017.

The authors are with the Department of Industrial and Information Engineering, Second University of Naples, Aversa 81031, Italy (e-mail: marco.balato@unina2.it; luigi.costanzo@unina2.it; pompeo.marino@unina2.it; guido.rubino@unina2.it; luigi.rubino@unina2.it; massimo.vitelli@unina2.it).

Color versions of one or more of the figures in this paper are available online at http://ieeexplore.ieee.org.

Digital Object Identifier 10.1109/JPHOTOV.2016.2634327

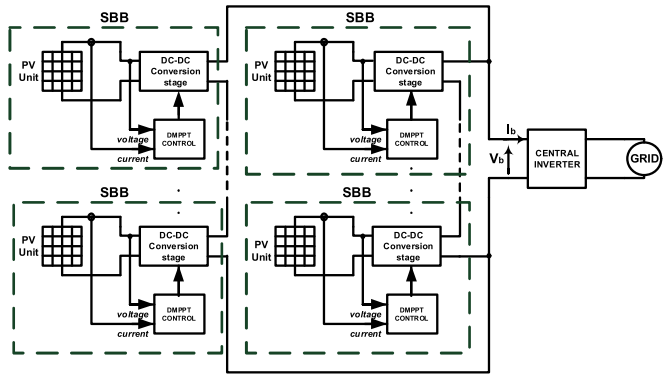

Fig. 1. Grid-connected PV system with DMPPT.

are based on the use of a number of dc–dc conversion stages that carry out the MPPT on as many PV Units (see Fig. 1). A PV unit can be a PV module, a submodule (e.g., half of a PV module), or a group of an arbitrarily small number of PV cells [7]–[15]. In the following, the term string building block (SBB) will be used to identify the set that is composed by a PV unit and by its associated dc–dc conversion stage (see Fig. 1). Strings of SBBs can be put in parallel in order to feed the central inverter (see Fig. 1). The MPPT technique TEODI is an example of the analog MPPT technique that is suitable for DMPPT PV applications and that can be applied to PV units of arbitrarily small size [12]–[15].

It is worth noting that DMPPT architectures efficiently work in mismatching conditions only if such mismatching conditions occur among different PV units and not inside the same PV unit. As a consequence, it is clear that, in order to decrease the probability of occurrence of mismatching conditions inside the same PV unit, it is convenient that each PV unit is relatively small. Of course, the choice of the size of the PV units must be made on the basis of a suitable compromise between economic cost and desired efficiency performances (in mismatching conditions) of the overall PV system. The lower the size of the PV Units, the lower the probability of occurrence of mismatching conditions inside the same PV unit, but the higher the economic cost of the whole PV system. In order to avoid the adoption of too small PV units, it is, therefore, necessary to improve the performances of the MPPT techniques that are usually implemented in the SBBs. In fact, if mismatching conditions occur inside the same PV unit, nearly all the standard MPPT techniques may fail [1]. As a consequence, it is necessary to modify

a given original MPPT technique in order to obtain a more efficient working of its modified version in the case of mismatching conditions that occur inside the same PV unit. As an example, under mismatching conditions, in order to avoid the failure of the Perturb and Observe (P&O) technique [16], it is mandatory to carry out a more-or-less rough periodic scan of the *P–V* characteristic of the PV unit in order to identify the region where the MPP is located. Afterward, the exact MPP position can be accurately found by means of the standard P&O algorithm [17]. It is worth noting that, in order to improve the performances of a given MPPT technique in mismatching conditions, it is usually necessary to accept both the worsening of the performances in uniform conditions and the increase of the complexity of the MPPT hardware control circuitry. As an example, always with reference to the P&O case, it is clear that during the periodic scan of the *P–V* characteristic, which is carried out by the grid-connected inverter, since the operating point of the PV array is more or less far from the MPP, the extracted energy is considerably lower than that theoretically available [17]. Moreover, in uniform conditions, the energy that can be extracted by means of the original P&O technique is higher than the corresponding energy that can be extracted by means of the modified P&O technique. Furthermore, in order to carry out the scan, it is of course necessary to use additional hardware components.

Similar considerations also hold for whichever MPPT technique. In particular, in this paper, the focus is on the TEODI technique [12]–[15]. After a brief resume of the working principle of TEODI in Section II, the modifications that are necessary in order to get the correct working of the modified TEODI (MTEODI) technique, in mismatching conditions, are deeply discussed in Section III. Section IV is devoted to the analysis of the experimental results that confirm the validity of the proposed MTEODI technique.

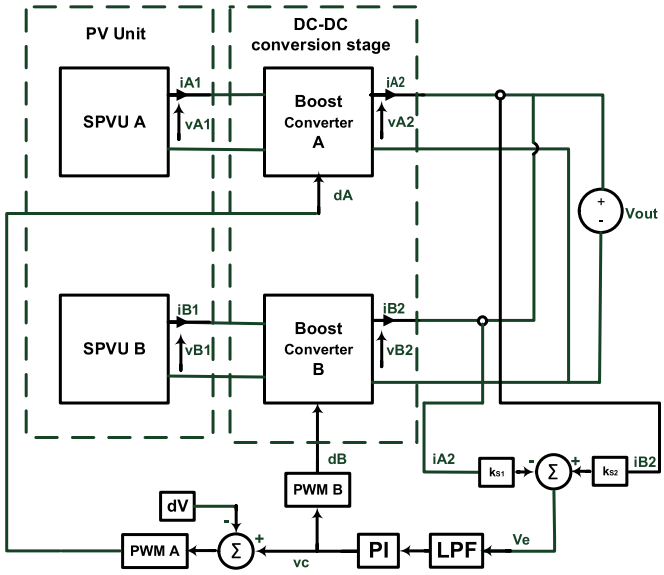

Fig. 2. Schematic representation of the operating principle of TEODI ($k_{S1} = k_{S2} = 1$) and MTEODI ($k_{S1} \geq 1, k_{S2} \geq 1$).

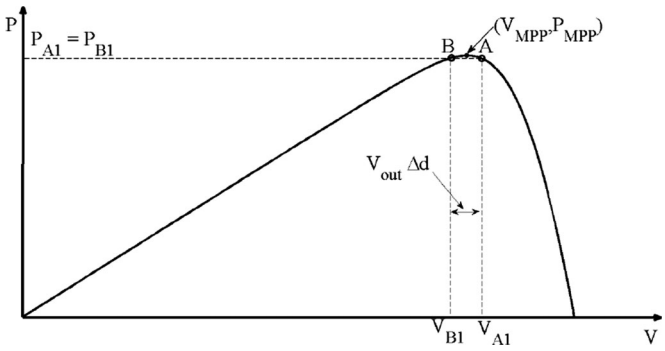

Fig. 3. *P–V* characteristic of each SPVU.

II. TEODI Technique

A. Working of TEODI in Uniform Operating Conditions

The basic TEODI SBB (TSBB) is shown in Fig. 2. The PV unit is composed of two identical subsections (SPVUs). The dc–dc conversion stage is composed of two dc–dc converters; each converter is fed by its own SPVU. In the following, without any loss of generality, the boost topology will be considered for both the dc–dc converters. The output ports of the two boost converters are connected in parallel (see Fig. 2). For the sake of simplicity of explanation, losses taking place in the power stage of the boost dc–dc converters (conduction losses, switching losses, iron losses, etc.) or in connecting cables will be neglected. The MPPT technique TEODI is based on the equalization of the output powers of the two boost converters in correspondence of a forced displacement of their input voltages [12]–[15]. The working principle of TEODI is based on the following conditions:

$$I_{A2} = I_{B2} \tag{1}$$

$$d_A = d_B - \Delta d \tag{2}$$

where $I_{\mathrm{A}2}$ and $I_{\mathrm{B}2}$ are the dc output currents of boost converters A and B, respectively (see Fig. 2); d_{A} and d_{B} are the time-varying values of the duty-cycle signals driving the switches of boost converters A and B, respectively; Δd is a constant value equal to dV/V_{s} $(0 < \Delta d < 1)$; V_{s} is the peak amplitude of the saw-tooth carrier waveforms of the two pulse width modulation (PWM) modulators; and dV is a constant voltage offset (see Fig. 2).

The choice of dV must be made on the basis of a reasonable compromise between steady-state MPPT efficiency and dynamic performances of the PV system [12]–[15]. In absence of mismatching conditions between the two SPVUs, their *P–V* characteristics are nearly coincident (see Fig. 3). The fulfillment of (1) is due to the action of the proportional–integral (PI) controller of Fig. 2. The fulfillment of (2) is obtained by simply subtracting dV from the output of the PI controller in order to provide two different input signals to the two PWM modulators of Fig. 2. As shown in Fig. 3, at the steady state, the operating points of the two SPVUs are located at the opposite sides with respect to the MPP voltage V_{MPP} (Points A and B) [12]–[15]. In fact, since $V_{\mathrm{A}2} = V_{\mathrm{B}2} = V_{\mathrm{out}}$ and $I_{\mathrm{A}2} = I_{\mathrm{B}2}$, then

$$P_{\mathrm{A}2} = P_{\mathrm{B}2} \tag{3}$$

where $V_{\mathrm{A}2}$ and $V_{\mathrm{B}2}$ ($P_{\mathrm{A}2}$ and $P_{\mathrm{B}2}$) are the dc output voltages (powers) of boost converters A and B, respectively. From (2)

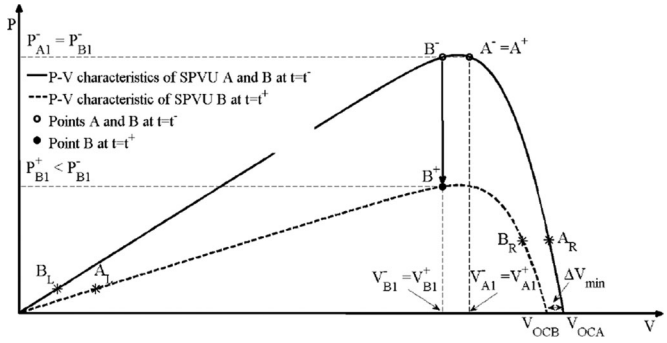

Fig. 4. *P–V* characteristics of the two SPVUs.

and (3), we obtain

$$P_{A1} = P_{B1} \tag{4}$$

$$V_{A1} = V_{B1} + V_{\text{out}} \cdot \Delta d \tag{5}$$

where V_{A1} and V_{B1} (P_{A1} and P_{B1}) are the dc input voltages (powers) of boost converters A and B, respectively. Equation (5) clearly shows that, at the steady state, the smaller the value of *dV* (and hence of Δd), the smaller the displacement of the operating point of each SPVU from the MPP, and therefore, the higher the steady-state MPPT efficiency. The main advantages of TEODI are represented by the simplicity of implementation, the absence of memory and multiplication operations, and the high MPPT efficiency.

B. Working of TEODI in Mismatching Operating Conditions

However, as discussed in detail in [12]–[15], such a high MPPT efficiency is obtainable only if the two SPVUs of a given TSBB work in uniform irradiance conditions, that is, as discussed in Section I, the correct working of a DMPPT PV system adopting TEODI is obtained only if mismatching conditions occur among different TSBBs and not inside the same TSBB. In order to describe the behavior of TEODI in mismatching conditions, let us suppose that at $t = t^-$, SPVUs A and B, as shown in Fig. 4, work in points A^- and B^-, respectively, since no mismatching conditions have occurred. Moreover, let us suppose that at $t = t^+$, due to the occurrence of an arbitrary mismatching event, the *P–V* characteristic of SPVU B changes and becomes the dotted curve of Fig. 4, that is, at $t = t^+$, the irradiance level of SPVU B is supposed to become lower than the irradiance level of SPVU A. At $t = t^+$, the operating point of SPVU B changes from B^- to B^+, while the operating point of SPVU A does not change ($\text{A}^+ = \text{A}^-$). It is

$$P_{B2}^+ = P_{B1}^+ < P_{A1}^+ = P_{A2}^+ = P_{A1}^- = P_{A2}^- \tag{6}$$

where P_{A1}^- and P_{B1}^- (P_{A1}^+ and P_{B1}^+) are the output powers of SPVUs A and B, respectively, at $t = t^-$ ($t = t^+$). As a consequence of (6), at $t = t^+$, $I_{B2}^+ < I_{A2}^+$, and then, the error signal V_e^+ (see Fig. 2) at the input of the PI controller becomes negative. Therefore, at $t = t^+$, d_{B} and d_{A} begin to decrease; they continue to decrease until $P_{\text{B1}} < P_{\text{A1}}$. Since the output voltage V_{out} is fixed, both input voltages v_{A1} and v_{B1} begin to increase; they continue to increase until $P_{\text{B1}} < P_{\text{A1}}$. Hence, the operating points of the two SPVUs begin to drift away from the corresponding MPPs. In conclusion, the occurrence of the considered mismatching event is able to induce TEODI in error, since there is no certainty that a new steady-state equilibrium condition is found. In practice, depending on the adopted value of Δd and on the degree of mismatching existing between the two SPVUs A and B, the following case can take place: $S_{\text{A}} > S_{\text{B}}$ and $V_{\text{out}} \cdot \Delta d < (V_{\text{OCA}} - V_{\text{OCB}}) = \Delta V_{\text{min}}$ (V_{OCA} is the open-circuit voltage of SPVU A, and V_{OCB} is the open-circuit voltage of SPVU B). In such a case, the two operating voltages V_{A1} and V_{B1}, placed at a distance $V_{\text{out}} \cdot \Delta d$, and characterized by the same level of the PV power, do not exist at all (see Fig. 4). Hence, the behavior of the system would be unstable because it would not be able at all to find an equilibrium point. Moreover, if such a steady-state equilibrium condition is found, it is obviously characterized by a quite low extracted power, since the steady-state operating points of both the SPVUs will be located more or less far and on the right of the MPP (points A_{R} and B_{R} of Fig. 4). Similar considerations can be drawn in case the mismatching event is such that, at t^+, the irradiance level of SPVU A is lower than the irradiance level of SPVU B. In such a case, if a steady-state equilibrium condition is found, the operating points of both the SPVUs will be located more or less far and on the left of the MPP (points A_{L} and B_{L} of Fig. 4).

III. Modified TEODI Technique

The objective of this section is to discuss a proper modification of TEODI that is able to lead to the efficient working of the MPPT even when mismatching conditions occur inside the same TSBB. Such a technique will be named MTEODI technique. MTEODI is based on the periodic measurement of the short-circuit currents of the two SPVUs. The knowledge of such currents allows not only to determine if mismatching conditions occur, but also to identify suitable correction factors k_{S1} and k_{S2}, on which the working of MTEODI is based. Since boost converters have been considered, short-circuit conditions for the two SPVUs are simply obtained by setting $d_{\text{A}} = d_{\text{B}} = 1$. In Fig. 2, the schematic representation of the operating principle of MTEODI is shown. The main difference between TEODI and MTEODI, apart the need to periodically measure the SPVU short-circuit currents, is represented by the expression of the error signal at the input of the PI controller. In particular, in the case of TEODI, being the two *k* factors (k_{S1} and k_{S2}) always equal to 1, the corresponding error signal v_{e} is equal to

$$v_e = i_{B2} - i_{A2}. \tag{7}$$

Instead, in the case of MTEODI, the error signal v_{e} at the input of the PI controller is equal to

$$v_e = k_{S2} \cdot i_{B2} - k_{S1} \cdot i_{A2}. \tag{8}$$

In practice, the error signal v_{e} that is adopted in TEODI is corrected in MTEODI by means of the correction factors k_{S1} and k_{S2}. It is evident that, in uniform irradiance conditions, we must have $k_{\text{S1}} = k_{\text{S2}} = 1$, since TEODI needs no correction when no mismatching conditions occur. In the following, always

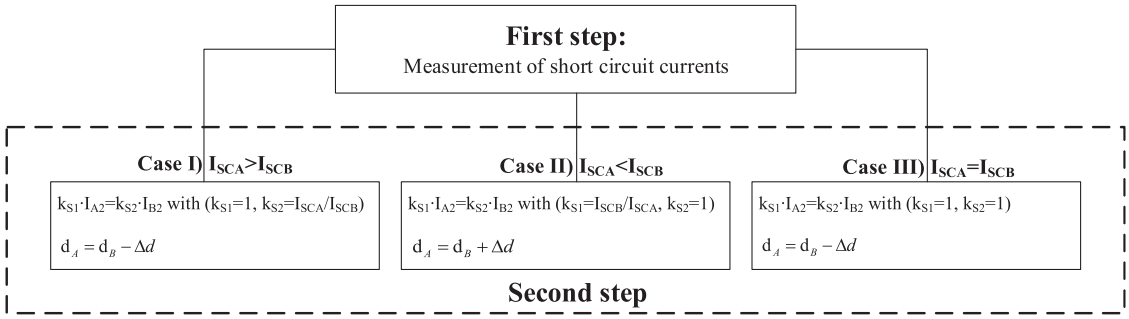

Fig. 5. Flowchart of MTEODI.

with reference to the example shown in Fig. 4, the guidelines concerning the evaluation of $k_{\rm S1}$ and $k_{\rm S2}$ are provided.

A. Guidelines for the Evaluation of the Correction Factors

The main objective is to obtain that, in mismatching conditions, the steady-state values of $v_{\rm A1}$ and $v_{\rm B1}$ remain nearly equal to V_{A1}^{-} and V_{B1}^{-}, respectively. This way, the overall efficiency of the MPPT function can be kept high, since, even in mismatching conditions, the steady-state operating points do not drift away from the corresponding MPPs. In order to obtain such an objective, at $t = t^{+}$ (i.e., when mismatching condition occurs), the error signal of MTEODI must be nearly equal to zero, even though $I_{\rm B2}^{+} \leq I_{\rm A2}^{+}$, that is

$$V_e^{+} = k_{S2} \cdot {I_{B2}}^{+} - k_{S1} \cdot {I_{A2}}^{+} = 0. \tag{9}$$

This means that the values of $k_{\rm S1}$ and $k_{\rm S2}$ must be chosen in order to compensate the difference existing at $t = t^{+}$ between the output currents of the two dc–dc converters; such a difference is due to the occurrence of the mismatching conditions. In particular, we have

$$k_{S2} = \frac{{I_{A2}}^{+}}{{I_{B2}}^{+}} \tag{10}$$

$$k_{S1} = 1 \tag{11}$$

where

$$\frac{{I_{A2}}^{+}}{{I_{B2}}^{+}} = \frac{{P_{A2}}^{+}}{{P_{B2}}^{+}} = \frac{{P_{A1}}^{+}}{{P_{B1}}^{+}} = \frac{{P_{A1}}^{-}}{{P_{B1}}^{+}} = \frac{{P_{B1}}^{-}}{{P_{B1}}^{+}} = \frac{I_{B1}^{-}}{{I_{B1}}^{+}}. \tag{12}$$

It is worth noting that, if the operating point of SPVU B is located at the left of its MPP both at t^{-} and at t^{+}, due to the nearly flat shape of the current versus voltage PV characteristic at the left of the MPP, with very good approximation, it is possible to state that

$$k_{S2} = \frac{{I_{B1}}^{-}}{{I_{B1}}^{+}} = \frac{{I_{\rm SCB}}^{-}}{{I_{\rm SCB}}^{+}} = \frac{{I_{\rm SCA}}^{-}}{{I_{\rm SCB}}^{+}} = \frac{{I_{\rm SCA}}^{+}}{{I_{\rm SCB}}^{+}} \tag{13}$$

where $I_{\rm SCA}$ and $I_{\rm SCB}$ are the short-circuit currents of SPVUs A and B, respectively. Equation (13) allows us to state that, in the considered mismatching condition, $k_{\rm S2}$ must be equal to the ratio between the short-circuit currents ${I_{\rm SCA}}^{+}$ of SPVU A and ${I_{\rm SCB}}^{+}$ of SPVU B, at $t = t^{+}$. It is worth noting that, in order to correctly operate, MTEODI needs to keep the operating point of the SPVU that is characterized by the highest power (A in the considered example) at the right of the corresponding MPP (in nearly the same location obtained with TEODI). Moreover, in order to correctly operate, MTEODI needs to keep the operating point of the SPVU that is characterized by the lowest power (B in the considered example) at the left of the corresponding MPP. It is also worth noting that, if the irradiance levels are time varying, the short-circuit current values are time varying as well. Hence, the higher the speed of variation of the irradiance levels, the higher the MTEODI required frequency of measurement of the short-circuit currents, that is, the MTEODI required frequency of update of the correction factors $k_{\rm S1}$ and $k_{\rm S2}$.

On the basis of the above discussion, it is possible to write the equations that describe the working principle of MTEODI

$$k_{S1} = 1,\ k_{S2} = \frac{I_{\rm SCA}}{I_{\rm SCB}} \tag{14}$$

$$d_A = d_B - \Delta d \tag{15}$$

when ${I_{B1}}^{+} < {I_{B1}}^{-}$. Instead

$$k_{S1} = \frac{I_{\rm SCB}}{I_{\rm SCA}},\ k_{S2} = 1 \tag{16}$$

$$d_A = d_B + \Delta d \tag{17}$$

when $I_{A1}^{+} < I_{A1}^{-}$.

Equations (15) and (17) are valid provided that the adopted dc/dc converters exhibit a conversion ratio that is a growing function of the duty cycle (e.g., boost, buck, buck–boost, SEPIC, Cuk, etc.). As shown by (15) and (17), with MTEODI, the duty cycle $d_{\rm A}$ can be lower or higher than $d_{\rm B}$ (instead with TEODI, it is always $d_{\rm A} < d_{\rm B}$). This is due to the fact that, as discussed above, in order to get the correct working of MTEODI, the operating point of the SPVU that is characterized by the highest irradiance level must be located on the right of the corresponding MPP. Instead, the operating point of the SPVU that is characterized by the lowest irradiance level must be located on the left of the corresponding MPP. Therefore, the magnitude of $d_{\rm A}$ with respect to that of $d_{\rm B}$ strictly depends on which is the greatest one between the irradiance levels of SPVU A and of SPVU B.

In fact, when mismatching occurs, if $S_{\rm A} \geq S_{\rm B}$ and, hence, $I_{\rm SCA} \geq I_{\rm SCB}$, then (15) is valid (see also Fig. 5). Instead, if $S_{\rm A} < S_{\rm B}$ and hence $I_{\rm SCA} < I_{\rm SCB}$, then (17) is valid (see also Fig. 5). The working principle of MTEODI is summarized in Fig. 5, in which the flowchart of such a technique is reported. The first step of MTEODI is represented by the measurement

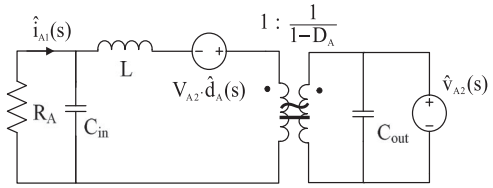

Fig. 6. Small-signal low-frequency equivalent circuit of subsystem A.

of the short-circuit currents of the two SPVUs. Such a measurement must be periodic with period T^*. The knowledge of I_{SCA} and I_{SCB} allows us to determine if the two SPVUs work in mismatching conditions (Cases I and II) or not (Case III). Once the working case is identified, it is possible to evaluate not only the factors k_{S1} and k_{S2}, but also the correct set of equations to adopt. As shown in the following section, in mismatching conditions, MTEODI allows us to obtain a considerable increase of the energetic efficiency with respect to TEODI. It is quite obvious that the higher $f^* = 1/T^*$, the higher the speed of variation of mismatching conditions which can be efficiently faced by MTEODI. On the other hand, the higher f^*, the higher the waste of energy occurring during each measurement interval. During each measurement interval, in order to measure I_{SCA} and I_{SCB}, the SPVUs are forced to operate in short-circuit conditions (that is why they are not able to provide power). After setting the duty cycles of the two boost dc-dc converters nearly equal to 1, it is necessary to wait for an enough long time interval in order to get steady-state conditions; only at this point (steady-state conditions), it is possible to measure the short-circuit currents. Of course, the choice of the measurement interval depends on the specific PV system under consideration. In fact, the measurement interval must be greater than the settling time T_{s} of the step response of a well-defined transfer function (G_{id}) of the specific PV system under consideration. G_{id} is the small-signal transfer function between the duty cycle and the PV current. The expression of such a transfer function can be easily found by analyzing the small-signal low-frequency equivalent circuit [1] of the subsystem that is composed by the SPVU, the boost converter, and the load. In the following, for the sake of simplicity, reference will be made to subsystem A. Results can be easily extended to subsystem B. The small-signal low-frequency equivalent circuit of subsystem A is reported in Fig. 6 [1].

Hat symbols indicate small-signal low-frequency variations [1] of the corresponding variables. The resistance R_{A} in Fig. 5 is the differential resistance of SPVU A [1]

$$R_A = \frac{V_{\mathrm{MPPA}}}{I_{\mathrm{MPPA}}}. \tag{18}$$

The expression of G_{id} for subsystem A is

$$G_{i_{A1}d_A} = \frac{\hat{i}_{A1}}{\hat{d}_A} = \frac{V_{A2}}{R_A}\cdot\frac{1}{s^2LC_{\mathrm{in}} + s\frac{L}{R_A} + 1}. \tag{19}$$

The settling time T_{s} of the step response of the above transfer function is equal to about 6 ms, if $V_{\mathrm{A2}} = 24$ V and the values of the remaining parameters are those ones of the test cases of Section IV (see Tables I and II).

TABLE I
ELECTRICAL CHARACTERISTICS OF EACH EMULATED SPVU IN STC

Open-circuit voltage	$V_{\mathrm{OC\_STC}} = 20.8$ V
Short-circuit current	$I_{\mathrm{SC\_STC}} = 3.0$ A
Maximum Power Point voltage	$V_{\mathrm{MPP\_STC}} = 15.9$ V
Maximum Power Point current	$I_{\mathrm{MPP\_STC}} = 2.7$ A
Voltage temperature coefficient	*alfa V* $= -0.34$%/K
Current temperature coefficient	*alfa I* $= 0.034$%/K

TABLE II
BOOST CONVERTER PARAMETERS

Power Inductor	$L = 180\ \mu$H
Power input Capacitor	$C_{\mathrm{in}} = 120\ \mu$F
Power output Capacitor	$C_{\mathrm{out}} = 220\ \mu$F
Switching frequency	$f_{\mathrm{S}} = 10$ kHz

IV. EXPERIMENTAL RESULTS

In this section, the performances of MTEODI are compared with those ones of TEODI by analyzing different mismatching scenarios (MSs). In particular, a hardware-in-the-loop demonstrator (HILD) has been developed in order to test the performances of a TSBB. The proposed HILD, as shown in Fig. 7, is composed of three fundamental blocks: a PV emulation block that emulates the PV unit of the TSBB, the dc–dc conversion stage of the TSBB (two boost converters), and the energy storage block. The PV emulation block is composed of two dynamic field-programmable analog array (FPAA)-based PV emulators [18]–[19]. The adoption of PV emulators is necessary in order to be able to compare the performances of TEODI and MTEODI exactly in the same MSs. This is, of course, impossible to obtain by using real PV sources, due to the fact that the external climatic conditions are not under our control. As shown in Fig. 7, each PV emulator adopts a dc–dc power supply whose output current is regulated by means of a proper FPAA-based controller. The adopted power supply is a Kepco BOP 36-12M (KBOP) [20], which is a device that is able to operate in all four quadrants of the current voltage plane. It is a linear power supply with two bipolar selectable control channels (voltage or current mode) that are individually controllable either by front panel controls (front panel voltage or front panel current control mode) or by remote control signals (remote voltage or remote current control mode). In the considered application, each KBOP works in remote current control mode. The control signals ($i_{\mathrm{A1\_ref}}(t)$ and $i_{\mathrm{B1\_ref}}(t)$) of the two KBOPs are generated by as many FPAAs [21]. In each FPAA, the nonlinear equation $I = f(I,V)$ that describes the *I–V* curve of the desired PV module has been implemented [18], [19]. Therefore, in each FPAA, a set of seven parameters has been uploaded by means of the "Anadigm designer 2" programming tool [18]–[19]: STC short-circuit current ($I_{\mathrm{SC\_STC}}$), STC open-circuit voltage ($V_{\mathrm{OC\_STC}}$), STC MPP voltage and current ($V_{\mathrm{MPP\_STC}}$ and $I_{\mathrm{MPP\_STC}}$), and voltage and current temperature coefficients *alfaV* ([%/K]) and *alfaI* ([%/K]). In particular, the electrical parameters of the two emulated SPVUs are reported in Table I. As far as SPVU A (B) is concerned, the corresponding FPAA input signals (see Fig. 7)

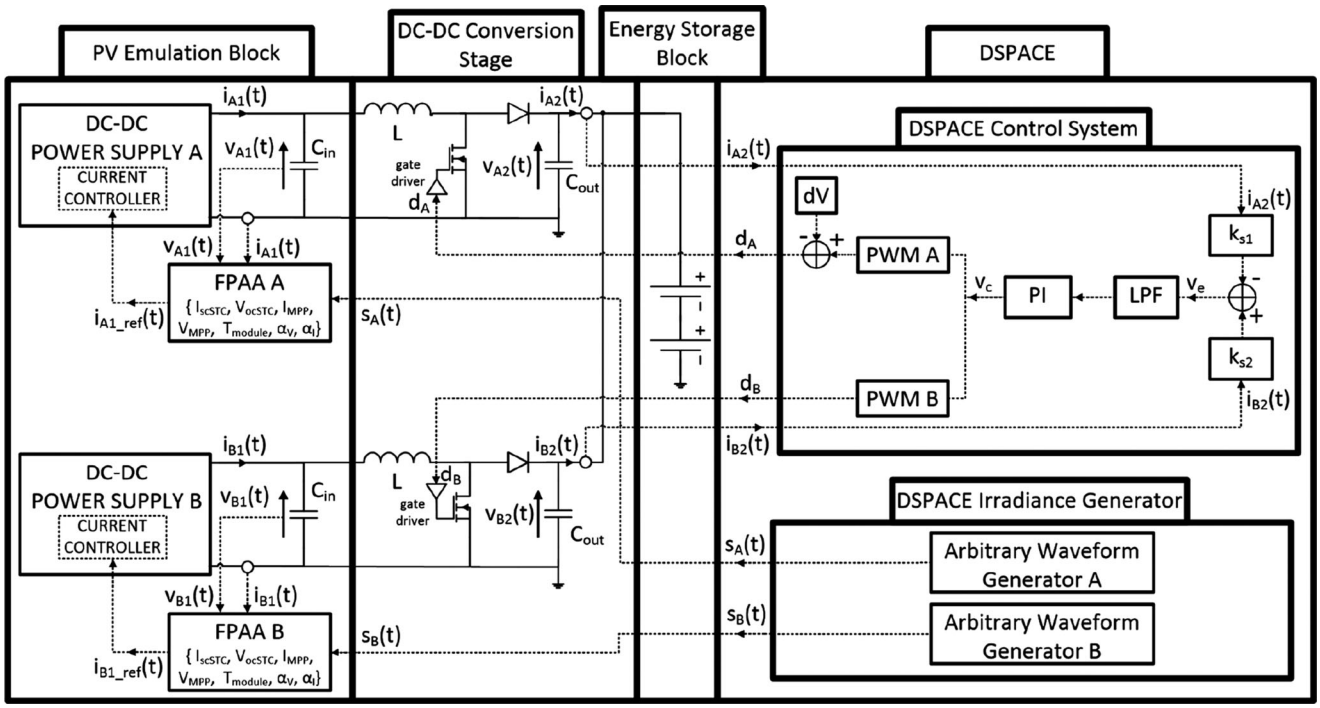

Fig. 7. Hardware-in-the-loop demonstrator.

are the following: the KBOP output current $i_{\mathrm{A}1}(t)\,(i_{\mathrm{B}1}(t))$, the KBOP output voltage $v_{\mathrm{A}1}(t)\,(v_{\mathrm{B}1}(t))$, and the time-varying signal $S_{\mathrm{A}}(t)\,(S_{\mathrm{B}}(t))$ that is proportional to the desired time-varying irradiance profile. The two signals $S_{\mathrm{A}}(t)$ and $S_{\mathrm{B}}(t)$ have been generated by means of a dSPACE DS1104 controller board [22] with the help of MATLAB/Simulink software. TEODI and MTEODI have been implemented in the same dSPACE DS1104 board. As concerns the dc–dc conversion stage, the values of the main parameters of the two boost dc–dc converters are reported in Table II.

The chosen switching frequency (10 kHz) is quite low with respect to the values that are usually adopted in actual applications. The bottleneck is represented by the adopted dSPACE board [22] that does not allow the adoption of higher switching frequencies. In any case, it is worth noting that the aim of the following experimental tests is only that of providing a "proof of concept" of the correct working of the proposed MPPT algorithm (MTEODI) in mismatching conditions. The adoption of higher switching frequencies can only be beneficial for the proposed MPPT technique due to the occurrence of lower switching currents and voltages ripples (higher steady-state MPPT efficiency) and due to a faster dynamics (lower values of the filter components of the power stage) of the MPPT control (higher MPPT dynamic efficiency). In conclusion, it can be stated that the actual performances of the proposed MPPT technique (steady-state and dynamic efficiency) can only be improved by the adoption of switching frequencies that are higher than 10 kHz.

As concerns the energy storage block, it is composed of the series connection of two EXIDE Excell EB440A lead-acid batteries that are 12 V 44 Ah. All the data and experimental results have been acquired and displayed by means of a Tektronix oscilloscope (Tektronix TDS 5054). The remaining parameters of the control circuitry are reported in Table III.

TABLE III
CONTROL CIRCUITRY PARAMETERS

Δd	0.02
PI controller	$G_{\mathrm{c}}(\mathrm{s}) = (2.5{\cdot}10^{-6}\mathrm{s} + 0.059)/(5{\cdot}10^{-5}\mathrm{s})$
Low-Pass Filter	$\mathrm{LP(s)} = 1/(2.53{\cdot}10^{-10}\ \mathrm{s}^2 + 2.228{\cdot}10^{-5}\ \mathrm{s} + 1)$
V_{s}	1

A. First Test Case

The first considered MS is characterized by the two irradiance signals $S_{\mathrm{A}}(t)$ and $S_{\mathrm{B}}(t)$ that are shown in Fig. 8. The signal $S_{\mathrm{A}}(t)$ assumes a constant value equal to 2.8 V, which corresponds to an irradiance level equal to 1000 W/m^2. Instead, the signal $S_{\mathrm{B}}(t)$ is a periodic square wave signal (period $T_{\mathrm{p}} = 100$ s, duty cycle $= 0.5$) with a lower value equal to 1.68 V (600 W/m^2) and a higher value equal to 2.8 V (1000 W/m^2). In practice, the TSBB initially operates in uniform conditions (1000–1000 W/m^2); after $T_{\mathrm{p}}/2$ s, mismatching conditions occur (1000 − 600 W/m^2). The TSBB remains in such stationary mismatching conditions for other $T_{\mathrm{p}}/2$ s, and afterward, the cycle uniform-mismatching conditions repeats again. In Fig. 9, the experimental results that have been obtained by using TEODI are reported. As expected, when mismatching conditions occur at $T_{\mathrm{p}}/2$, the voltages of the two SPVUs begin to increase and a new steady-state condition is found on the right of the MPP. It is easy to understand that TEODI has been deceived since

Fig. 8. Time-domain behavior of $S_{\mathrm{A}}(t)$ and $S_{\mathrm{B}}(t)$. Time Base $M = 20$ s/div.

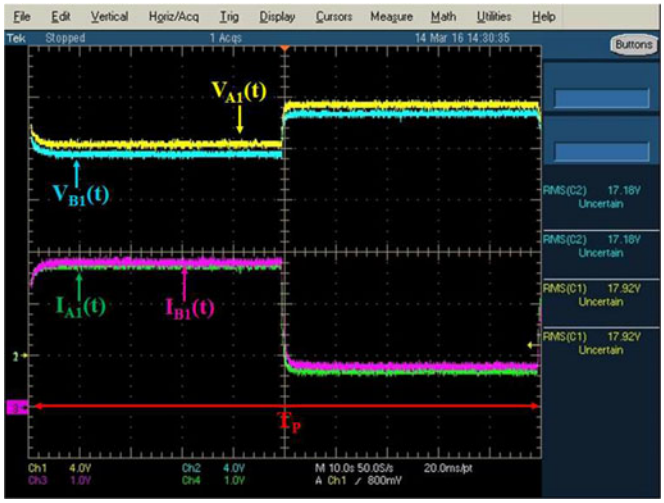

Fig. 9. Experimental results obtained by using TEODI: output voltage of SPVU A (yellow curve), output voltage of SPVU B (heavenly curve), output current of SPVU A (green curve), and output current of SPVU B (fuchsia curve). Time Base $M = 10$ s/div.

at least the operating point of SPVU A, for which the irradiance level has not changed, should remain nearly unchanged, in the new steady-state conditions. Instead, after the occurrence of mismatching conditions, in the new steady-state conditions, $V_{\mathrm{A}1}$ ($I_{\mathrm{A}1}$) assumes a higher (lower) value with respect to the corresponding old steady-state value. In Fig. 10, the experimental results that have been obtained by using MTEODI (with $T^* = T_{\mathrm{p}}/2$) are reported. In Fig. 11, the time-domain behavior of the two correction factors is shown.

As expected, in such a case, when mismatching conditions occur at $T_{\mathrm{p}}/2$, the voltages of the two SPVUs do not drift away from the MPP. Instead, they remain nearly unchanged. In such a case, it is evident from Fig. 10 that the operating voltage and the operating current of SPVU A, at the steady-state, before and after the occurrence of the mismatching conditions, assume nearly the same values. The only variable that, after $T_{\mathrm{p}}/2$, exhibits a strong variation (decrease) at the steady state is

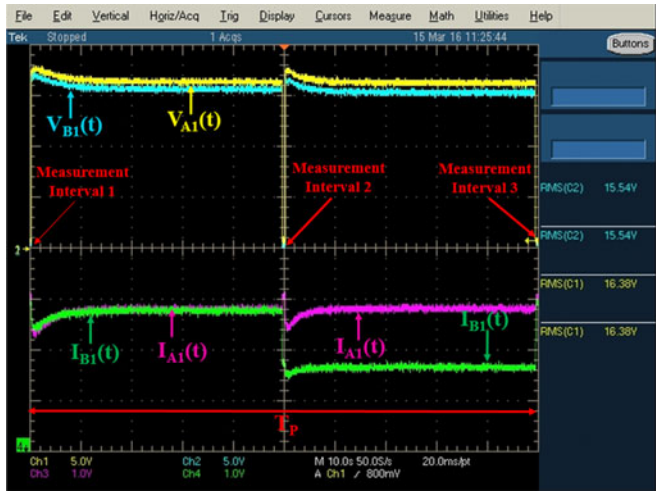

Fig. 10. Experimental results obtained by using MTEODI: output voltage of SPVU A (yellow curve), output voltage of SPVU B (heavenly curve), output current of SPVU A (fuchsia curve), output voltage of SPVU B (green curve). Time Base $M = 10$ s/div.

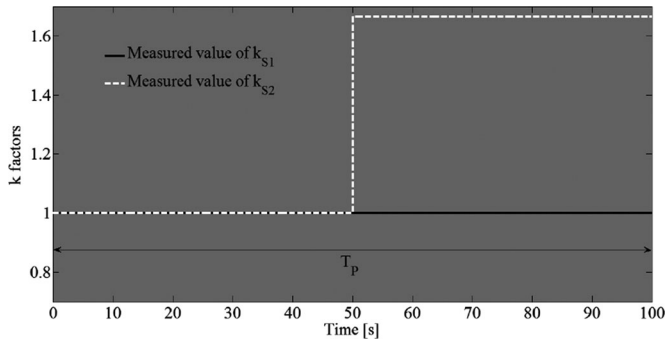

Fig. 11. Time-domain behavior of the two correction factors $k_{\mathrm{s}1}$ and $k_{\mathrm{s}2}$.

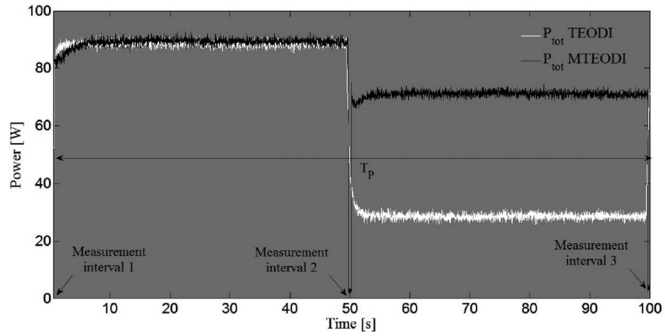

Fig. 12. Time-domain behavior of the total extracted powers.

the current of SPVU B. However, this is justified by the fact that the corresponding level of the irradiance (S_{B}) has been reduced by a factor of 0.6.

The time-domain behaviors of the total extracted powers when using TEODI and MTEODI are shown in Fig. 12. From the analysis of Fig. 12, it is evident that, in uniform operating conditions, as expected, the energetic efficiency of both techniques is the same because, under uniform irradiance con-

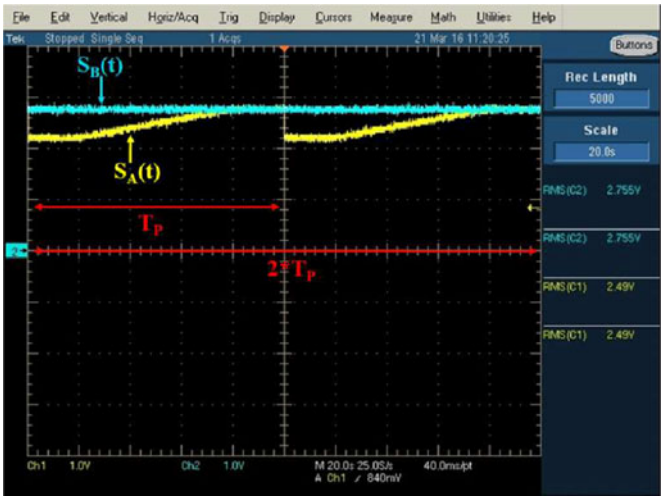

Fig. 13. Time-domain behavior of S_A (t) and S_B (t). Time Base $M = 20$ s/div.

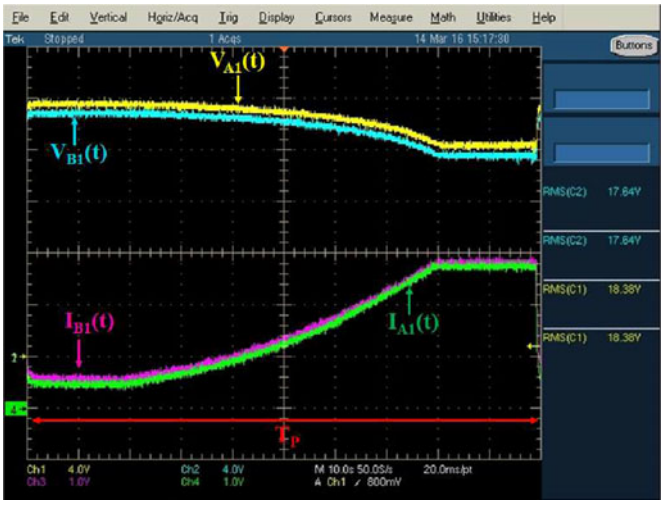

Fig. 14. Experimental results obtained by using TEODI: output voltage of SPVU A (yellow curve), output voltage of SPVU B (heavenly curve), output current of SPVU A (green curve), and output voltage of SPVU B (fuchsia curve). Time Base $M = 10$ s/div.

ditions, MTEODI is perfectly coincident with TEODI. When instead mismatching conditions occur, MTEODI outperforms TEODI since this last is deceived.

B. Second Test Case

The second considered MS is characterized by the two irradiance signals $S_A(t)$ and $S_B(t)$ that are shown in Fig. 13. The signal $S_B(t)$ assumes a constant value equal to 2.8 V (1000 W/m^2). The signal $S_A(t)$ is instead a periodic signal (period $T_p = 100$ s). In the first part of the period ($t < T_p/5$), stationary mismatching conditions are emulated (1000–600 W/m^2). Instead, for $T_p/5 < t < 4T_p/5$, the degree of mismatching gradually reduces to zero. In the last part of the period ($4T_p/5 < t < T_p$), uniform operating conditions are emulated. The experimental waveforms that are shown in Fig. 14 refer to TEODI. Once again, it is easy to understand that TEODI has been

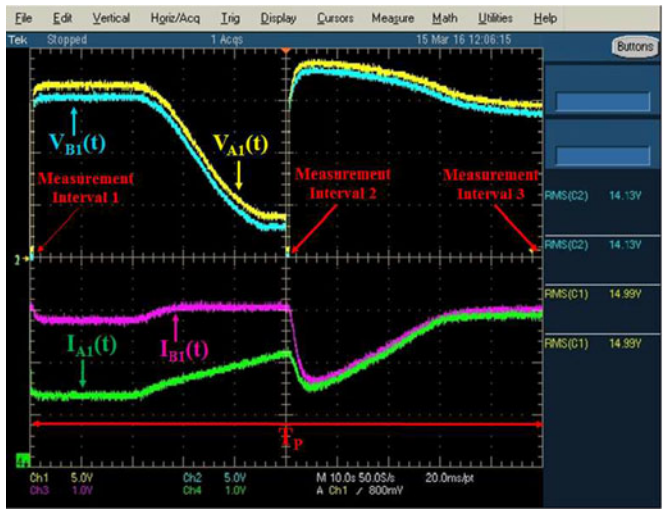

Fig. 15. Experimental results obtained by using MTEODI: output voltage of SPVU A (yellow curve), output voltage of SPVU B (heavenly curve), output current of SPVU A (green curve), and output voltage of SPVU B (fuchsia curve). Time Base $M = 10$ s/div.

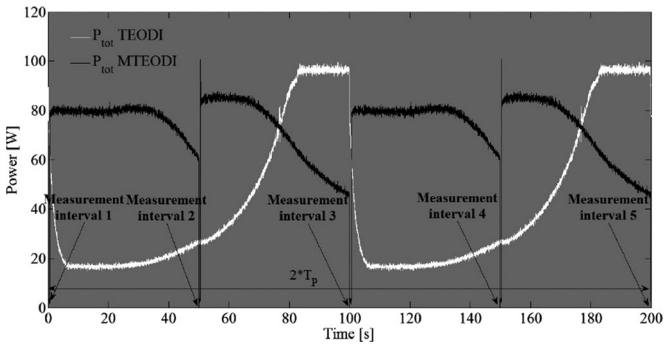

Fig. 16. Time-domain behavior of the total extracted powers.

deceived. In fact, the output current of SPVU B (for which the irradiance level is constant and high during T_p) reaches its MPP value only in the last part of the period ($4T_p/5 < t < T_p$), that is when no mismatching exists. This means that, at least SPVU B, in mismatching conditions ($t < 4T_p/5$) operates far from the MPP. The experimental waveforms that are shown in Fig. 15 refer to MTEODI. They put in evidence the important role that is played by the periodicity T^* of the short-circuit current measurement. In the case of Fig. 15, $T^* = T_p/2$. With such a choice, even if the average power that can be extracted by using MTEODI is higher than the average power that can be extracted by using TEODI (see Fig. 16), an interval of time exists where the instantaneous power that is extracted by using MTEODI is lower than the corresponding power that is extracted by using TEODI (see Fig. 16). This can be explained by considering that, for $0 < t < T^* = T_p/2$, MTEODI continues to use the values of k_{S1} and k_{S2} that have been detected at $t = 0$, when the first short-circuit current measurement takes place. Such values are right only for $0 < t < T_p/5$ since, for $T_p/5 < t < T^* = T_p/2$, mismatching conditions are time varying. As a consequence, for $T_p/5 < t < T^* = T_p/2$, the

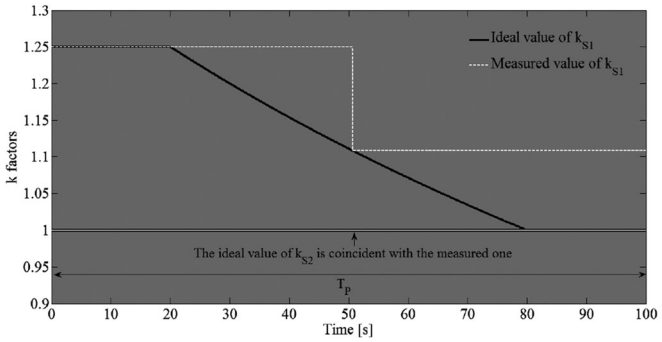

Fig. 17. Time-domain behavior of k_{s1} and k_{s2} ($T^* = T_p/2$).

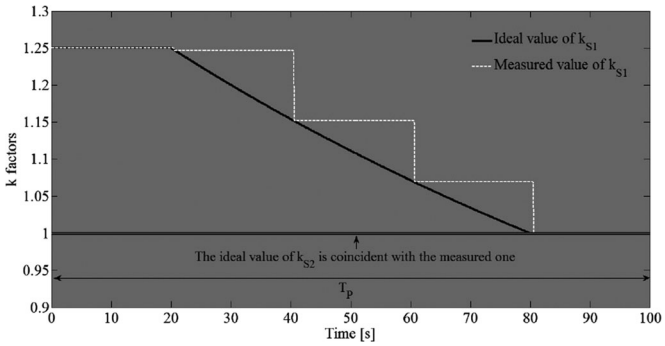

Fig. 18. Time-domain behavior of k_{s1} and k_{s2} ($T^* = T_p/5$).

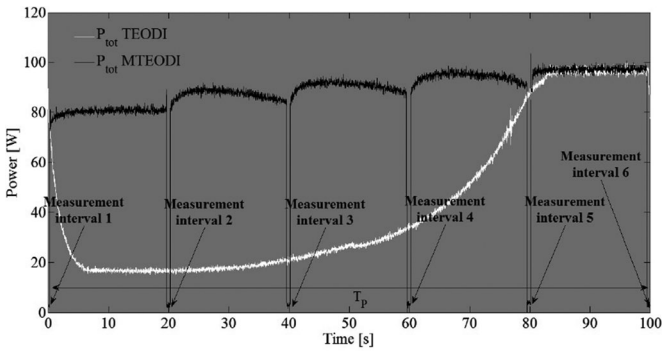

Fig. 19. Time-domain behavior of the total extracted powers.

correction of the error signal by means of k_{S1} and k_{S2}, that is, the core of MTEODI, is not exact. Similar considerations also hold with reference to the interval $T^* = T_p/2 < t < T_p$. In practice, $1/T^*$ represents the sampling frequency, with which the exact time-domain waveforms of k_{S1} and k_{S2} are sampled. The duration *T*' of the measurement interval can be considered negligible; *T*' must be large enough in order that steady-state input short-circuit conditions can settle in each dc–dc converter, but, of course, *T*' must be much lower than T^*. The hold time is just T^*. The above sampling process is represented in Figs. 17 ($T^* = T_p/2$) and 18 ($T^* = T_p/5$).

As expected, by adopting a higher measurement frequency ($T^* = T_p/5$), it is possible to improve the performances that can be obtained with MTEODI, as it is easy to understand by comparing Figs. 16 ($T^* = T_p/2$) and 19 ($T^* = T_p/5$).

V. Conclusion

The theoretical analysis and the experimental validation of the modified version of the MPPT technique TEODI have been presented and discussed. It has been shown that, since TEODI can be deceived by localized mismatching conditions, a proper modification is required in order to improve the MPPT performances when such localized mismatching conditions take place. Such a modification, which is based on the periodic measurement of the short-circuit currents of the two subsections of the PV unit, leads to the MTEODI technique. The experimental results clearly prove that when mismatching conditions occur, MTEODI allows us to obtain a considerable increase of the energetic efficiency if compared with TEODI, and therefore, they confirm the validity of the proposed approach.

References

[1] N. Femia, G. Petrone, G. Spagnuolo, and M. Vitelli, "*Power Electronics and Control Techniques for Maximum Energy Harvesting in Photovoltaic Systems*. Boca Raton, FL, USA, CRC, 2012.

[2] M. Balato, L. Costanzo, and M. Vitelli, "Maximum power point tracking techniques," in *Wiley Online Encyclopedia of Electrical and Electronics Engineering*. Hoboken, NJ, USA: Wiley, Feb. 2016, pp. 1–26.

[3] N. Femia, G. Lisi, G. Petrone, G. Spagnuolo, and M. Vitelli, "Distributed maximum power point tracking of photovoltaic arrays: Novel approach and system analysis," *IEEE Trans. Ind. Electron.*, vol. 55, no. 7, pp. 2610–2621, Jul. 2008.

[4] E. Roman, R. Alonso, P. Ibanez, D. Goitia, and S. Elorduizapatarietxe, "Intelligent PV module for grid-connected PV systems," *IEEE Trans. Ind. Electron.*, vol. 53, no. 4, pp. 1066–1073, Aug. 2006.

[5] W. Xiao, N. Ozog, and W.G. Dunford, "Topology study of photovoltaic interface for maximum power point tracking," *IEEE Trans. Ind. Electron.*, vol. 54, no. 3, pp. 1696–1704, Jun. 2007.

[6] G. R. Walker and P. C. Sernia, "Cascaded DC-DC converter connection of photovoltaic modules," *IEEE Trans. Power Electron.*, vol. 19, no. 4, pp. 1130–1139, Jul. 2004.

[7] R. Pilawa-Podgurski and D. Perreault, "Submodule integrated distributed maximum power point tracking for solar photovoltaic applications," *IEEE Trans. Power Electron.*, vol. 28, no. 6, pp. 2957–2967, Oct. 2013.

[8] J. Stauth, M. Seeman, and K. Kesarwani, "Resonant switched-capacitor converters for sub-module distributed photovoltaic power management," *IEEE Trans. Power Electron.*, vol. 28, no. 3, pp. 1189–1198, Mar. 2013.

[9] C. Olalla, D. Clement, M. Rodriguez, and D. Maksimovic, "Architectures and control of submodule integrated dc-dc converters for photovoltaic applications," *IEEE Trans. Power Electron.*, vol. 28, no. 6, pp. 2980–2997, Jun. 2013.

[10] S. Poshtkouhi, A. Biswas, and O. Trescases, "DC-DC converter for high granularity, sub-string MPPT in photovoltaic applications using a virtual-parallel connection," in *Proc. 27th Annu. IEEE Appl. Power Electron. Conf. Expo.*, Mar. 2012, pp. 86–92.

[11] S. Qin and R. C. N. Pilawa-Podgurski, "Sub-module differential power processing for photovoltaic applications," in *Proc. 28th Annu. IEEE Appl. Power Electron. Conf. Expo.*, May 2013, pp. 101–108.

[12] N. Femia, G. Petrone, G. Spagnuolo, and M. Vitelli, "A new analog MPPT technique: TEODI," *Prog. Photovoltaics, Res. Appl.*, vol. 18, no. 1, pp. 28–41, Jan. 2010.

[13] G. Petrone, G. Spagnuolo, and M. Vitelli, "An analog technique for distributed MPPT PV applications," *IEEE Trans. Ind. Electron.*, vol. 59, no. 12, pp. 4713–4722, Dec. 2012.

[14] M. Balato, L. Costanzo, P. Marino, L. Rubino, and M. Vitelli, "Dual implementation of the MPPT technique TEODI: Uniform and mismatching operating conditions," in *Proc. Int. Conf. Clean Elect. Power*, Aug. 2015, pp. 439–446.

[15] G. Petrone, G. Spagnuolo, and M. Vitelli, "TEODI: PV MPPT based on the equalization of the Output operating points in correspondence of a forced displacement of the input operating points," in *Proc. IEEE Int. Symp. Ind. Electron.*, Bari, Italy, Jul. 4–7, 2010, pp. 3463–3468.

[16] N. Femia, G. Petrone, G. Spagnuolo, and M. Vitelli, "Optimization of perturb and observe maximum power point tracking method," *IEEE Trans. Power Electron.*, vol. 20, no. 4, pp. 963–973, Jul. 2005.

[17] M. Balato and M. Vitelli, "Optimization of distributed maximum power point tracking PV applications: The scan of the power vs. voltage input characteristic of the inverter," *Int. J. Elect. Power Energy Syst.*, vol. 60, no. 1, pp. 334–346, Sep. 2014.
[18] F. Barra *et al.*, "Dynamic and reconfigurable photovoltaic emulator based on FPAA," in *Proc. 20th IMEKO TC4 Int. Symp.*, Benevento, Italy, Sep. 2014, pp. 1005–1010.
[19] M. Balato *et al.*, "Design and implementation of a dynamic FPAA based photovoltaic emulator," *Sol. Energy*, vol. 123, pp. 102–115, Jan. 2016.
[20] Kepco BOP 36-12M Datasheet, 2015. [Online]. Available: http://www.kepcopower.com/support/opmanls.htm#bop
[21] FPAA Datasheet, 2014. [Online]. Available: http://www.anadigm.com/an231e04.asp
[22] dSPACE DS1104 Controller Board Datasheet, 2016. [Online]. Available: http://www.dspace.com/en/inc/home/products/hw/singbord/ds1104.cfm

Marco Balato was born in Naples, Italy, in 1984. He received the M.Sc. degree in electronic engineering and the Ph.D. degree in energy conversion from the Second University of Naples (SUN), Aversa, Italy, in 2011 and 2014, respectively.

He is currently a Research Fellow with the Department of Industrial and Information Engineering, SUN. His main research interests include power electronics, modeling, and control techniques for energy conversion systems from renewable sources.

Luigi Costanzo was born in Villaricca (Napoli), Italy, in 1989. He received the master's degree (*cum laude*) in electronic engineering in 2014 from the Second University of Naples, Aversa, Italy, where he is currently working toward the Ph.D. degree in energy conversion with the Department of Industrial and Information Engineering.

His main research interests include power electronics, modeling, and control techniques for energy conversion systems from renewable sources; maximum power point tracking techniques in photovoltaic applications; power electronics circuits for renewable energy sources; methods for analysis and design of switching converters; and methods to harvest and store energy from any available source.

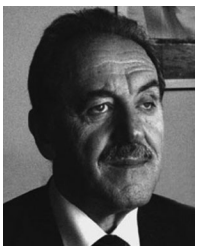

Pompeo Marino was born in Frosinone, Italy, on April 8, 1948. He received the M.Sc. degree in electronics engineering from the University of Naples "Federico II," Naples, Italy, in 1973.

He is a Professor in industrial electronics and electrical drives with the Department of Industrial and Information Engineering, Second University of Naples, Aversa, Italy. He is involved in research on electrical power system reliability and harmonic analysis. His interests include power converter design, ac and dc drives, and motion control.

Guido Rubino was born in Santa Maria Capua Vetere, Italy, in 1975. He received the M.Sc. degree in electronic engineering and the Ph.D. degree in energy conversion from the Second University of Naples (SUN), Aversa, Italy, in 2011 and 2014, respectively.

He is currently with the Department of Industrial and Information Engineering, SUN. Since 2009, he has been involved in several European projects in the aeronautical field (MOET project) and three CleanSky projects (I-primes, Mas De Nada, and Epocal). His research interests include energy conversion systems and power electronic converters for aeronautical and railway networks.

Luigi Rubino received the master's degree in electronic engineering and the Ph.D. degree in energy conversion from the Second University of Naples (SUN), Aversa, Italy, in May 2008 and 2012, respectively.

Since 2008, he has been involved in several European projects in the aeronautical field (MOET project, FP6), three CleanSky projects (I-primes, Mas De Nada, and Epocal), and many national projects. Since 2013, he has been an Assistant Professor with the Department of Mechanical and Information Engineering, SUN. Since 2015, he has been the Scientific Coordinator for the Department of Industrial and Information Engineering, SUN, of the Airbus-funded TUBA project, and, since January 2016, of the Clean Sky ASPIRE project. He is the author of more than 20 articles and two inventions. His research interests include power electronics, modeling, digital control, energy management, and power quality improvement.

Massimo Vitelli was born in Caserta, Italy, in 1967. He received the Laurea degree (*cum laude*) in electrical engineering from the University of Naples Federico II, Naples, Italy, in 1992.

He is currently a Full Professor with the Department of Industrial and Information Engineering, Second University of Naples, Aversa, Italy, where he teaches electrotechnics and power electronics. He is involved in many scientific national projects financed by the Italian Ministry of University and Research, by the Italian National Science Foundation, and by industry (C.R.I.S. Ansaldo, ELCON, MagneTek, Power One, Astrid Energy Enterprises, National Semiconductor Corporation, Elettronica Santerno, and Bitron). He is a coauthor of six national and international patents. His main research interests include maximum power point tracking techniques in photovoltaic applications; power electronics circuits for renewable energy sources; methods for analysis and design of switching converters; tolerance analysis/design of switching converters and in electromagnetic field problems by means of interval arithmetic, affine arithmetic, and genetic algorithms; and electromagnetic compatibility and electromagnetic characterization of new insulating and semiconducting materials. He was a Referee for the Committee for Evaluation of Research for the Italian Ministry of Education, University and Research of research products submitted for the evaluation of scientific research in Italy during 2001–2003.

Prof. Vitelli has been an Associate Editor of the IEEE TRANSACTIONS ON POWER ELECTRONICS since 2003. He was a Guest Editor for the IEEE TRANSACTIONS ON INDUSTRIAL ELECTRONICS—special section on "Industrial Electronics for Photovoltaic Systems" (2008), "Efficient and Reliable Photovoltaic Systems" (2008), and "Fuel Cells Power Processing and Control" (2009). He is a Component of the Technical Committee on Renewable Energy Systems of the IEEE Industrial Electronics Society and of the Power Electronics Technical Committee of the IEEE International Symposium on Circuits and Systems.